KRAKOWSKA
INTERDYSCYPLINARNA
SZKOŁA DOKTORSKA

Determination of the Proton Radius and Its Sensitivity to Photon-Induced Processes

Nikhil Krishna

Institute of Nuclear Physics, Krakow
Supervisors: dr.hab. Mariola Klusek Gawenda
dr. Rafal Staszewski

March 20, 2026

Outline

- Motivation: Understanding the proton's internal structure (charge radius)
- Electromagnetic form factors and radius extraction
- Photon-Photon interactions in proton-proton collision
- Momentum space Approach
- Impact parameter space Approach
- Effects of changing proton radius
- Rescattering corrections
- Experimental Sensitivity
- Summary

Proton Radius Puzzle

- Over the past 110 years, since its discovery, the proton has evolved

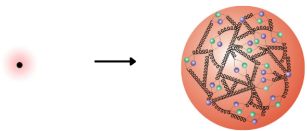

Figure: From point-like particle to composite particle made of quarks and gluons (QCD).

Proton Radius Puzzle

- Over the past 110 years, since its discovery, the proton has evolved

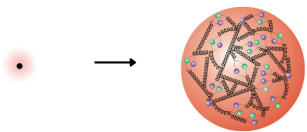

Figure: From point-like particle to composite particle made of quarks and gluons (QCD).

- Electromagnetic(charge) radius quantifies the distribution of charge within the proton.

Proton Radius Puzzle

- Over the past 110 years, since its discovery, the proton has evolved

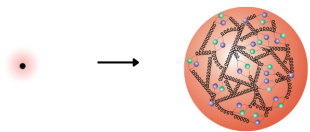

Figure: From point-like particle to composite particle made of quarks and gluons (QCD).

- Electromagnetic(charge) radius quantifies the distribution of charge within the proton.
- The "Proton Radius Puzzle" refers to disagreement between measurements from electron-proton scattering and hydrogen spectroscopy.

Proton Radius Puzzle

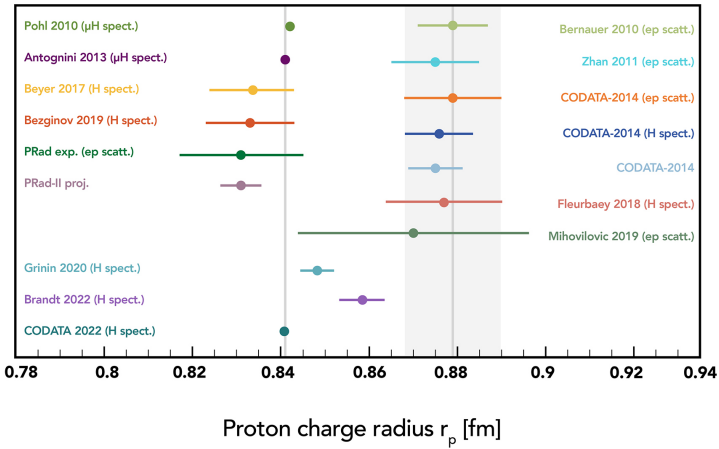

Figure: The proton charge radius determined from ep elastic scattering, spectroscopic experiments and world-data compilation from CODATA since 2010(ref:10.3390/universe9040182)

Proton-Proton Collision at LHC

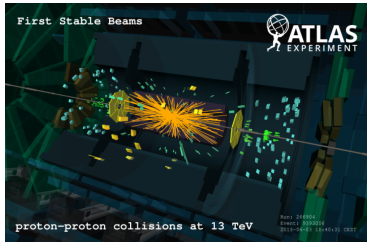

Figure: High energy proton collision at LHC producing numerous particles

Proton-Proton Collision at LHC

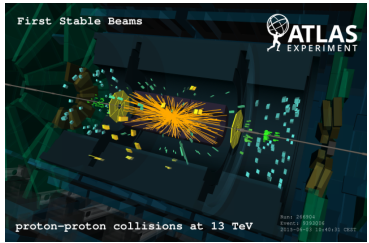

Figure: High energy proton collision at LHC producing numerous particles

- Significant fraction of p-p collision contains **quasi-real** photons- effectively can be treated as **Photon-Photon collision**.

Proton-Proton Collision at LHC

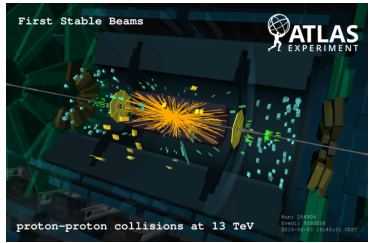

Figure: High energy proton collision at LHC producing numerous particles

- Significant fraction of p-p collision contains **quasi-real** photons- effectively can be treated as **Photon-Photon collision**.
- Studying these type of interactions in p-p collision gives information about photons from protons and enables calculating related cross sections. We primarily focus on exclusive lepton production processes.

Radius from Electromagnetic Form Factors

Form factors are Fourier transform of charge densities

$$F(Q^2) = \int \rho(r) e^{-q^2 r^2} d^3 r$$

Charge distribution	**Form factor**
$\rho(r) = \dfrac{\delta(r)}{4\pi r^2}$	$F_{\mathrm{pl}}(Q^2) = 1$
$\rho(r) = \left(\dfrac{\Lambda^2}{2\pi}\right)^{3/2} \exp\left(-\dfrac{\Lambda^2 r^2}{2}\right)$	$F_G(Q^2) = \exp\left(-\dfrac{Q^2}{2\Lambda^2}\right)$
$\rho(r) = \dfrac{\Lambda^3}{8\pi} \exp(-\Lambda r)$	$F_D(Q^2) = \left(1 + \dfrac{Q^2}{\Lambda^2}\right)^{-2}$

Table: Relation between charge distribution and form factors

Radius from Electromagnetic Form Factors

- The slope of the form factor at $Q^2 \to 0$ is used to extract the proton radius.

Radius from Electromagnetic Form Factors

- The slope of the form factor at $Q^2 \to 0$ is used to extract the proton radius.
- Taylor expanding the form factor and keeping only the lowest two terms:

$$F(Q^2) = 1 - \frac{1}{6} Q^2 \langle r^2 \rangle$$

$$\frac{dF(Q^2)}{dQ^2} = -\frac{\langle r^2 \rangle}{6}$$

$$\langle r^2 \rangle = -6 \frac{dF}{dQ^2}$$

Radius from Electromagnetic Form Factors

- The slope of the form factor at $Q^2 \to 0$ is used to extract the proton radius.
- Taylor expanding the form factor and keeping only the lowest two terms:

$$F(Q^2) = 1 - \frac{1}{6} Q^2 \langle r^2 \rangle$$

$$\frac{dF(Q^2)}{dQ^2} = -\frac{\langle r^2 \rangle}{6}$$

$$\langle r^2 \rangle = -6 \frac{dF}{dQ^2}$$

Form factor	**Radius**
$F_{\mathrm{pl}}(Q^2) = 1$	$r = 0\,\mathrm{fm}$
$F_G(Q^2) = \exp\left(-\frac{Q^2}{2\Lambda^2}\right)$	$r = 0.404\,\mathrm{fm}$
$F_D(Q^2) = \left(1 + \frac{Q^2}{\Lambda^2}\right)^{-2}$	$r = 0.809\,\mathrm{fm}$

Table: Proton radius for point-like, Gaussian, and dipole form factors; $\Lambda^2 = 0.71\,\mathrm{GeV}^2$.

Momentum Space Approach

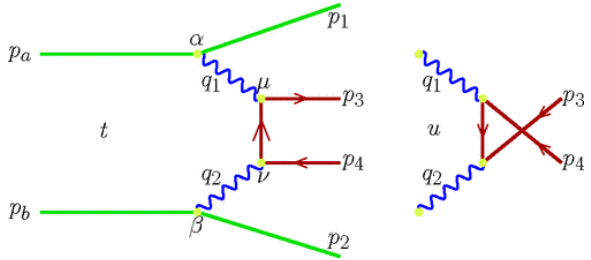

Figure: Photon-photon fusion interactions to the process $pp \to pp\,\ell^+\ell^-$: left – t-channel, right – u-channel.

- General form for the cross section can be written as:

$$\begin{aligned}\sigma &= \int \frac{1}{2s}\overline{|\mathcal{M}|^2}\,(2\pi)^4\,\delta^4\left(p_a + p_b - p_1 - p_2 - p_3 - p_4\right) \\ &\times \frac{d^3p_1}{(2\pi)^3\,2E_1}\,\frac{d^3p_2}{(2\pi)^3\,2E_2}\,\frac{d^3p_3}{(2\pi)^3\,2E_3}\,\frac{d^3p_4}{(2\pi)^3\,2E_4}\,. \end{aligned} \tag{1}$$

Momentum Space Approach

- Using the following transformation:

$$\frac{d^3p_i}{E_i} = dy_i\, d^2p_{i\perp} = dy_i p_{i\perp} dp_{i\perp} d\phi_i \tag{2}$$

- We can rewrite the cross section as,

$$\begin{aligned}\sigma &= \int \frac{1}{2s}\overline{|\mathcal{M}|^2}\delta^4\left(p_a + p_b - p_1 - p_2 - p_3 - p_4\right)\frac{1}{(2\pi)^8}\frac{1}{2^4} \\ &\times \left(dy_1 p_{1\perp} dp_{1\perp} d\phi_1\right)\left(dy_2 p_{2\perp} dp_{2\perp} d\phi_2\right)\left(dy_3 d^2p_{3\perp}\right)\left(dy_4 d^2p_{4\perp}\right)\ . \end{aligned} \tag{3}$$

where $p_{i\perp}$ are transverse momenta of outgoing protons and leptons in the final state, ϕ_1, ϕ_2 are azimuthal angles of the outgoing protons.

Momentum Space Approach

- Introducing new variable,

$$\mathbf{p}_{mt} = \mathbf{p}_{3t} - \mathbf{p}_{4t}$$

- Using 4-D Dirac delta function, cross section becomes,

$$\begin{aligned}\sigma &= \int \frac{1}{2s}\overline{|\mathcal{M}|^2}\delta\left(E_a + E_b - E_1 - E_2 - E_3 - E_4\right)\delta^3\left(p_{1z} + p_{2z} + p_{3z} + p_{4z}\right)\frac{1}{(2\pi)^8}\frac{1}{2^4} \\ &\times \left(dy_1 p_{1\perp} dp_{1\perp} d\phi_1\right)\left(dy_2 p_{2\perp} dp_{2\perp} d\phi_2\right) dy_3 dy_4 dp_m \; d\phi_{p_m} \,. \end{aligned} \tag{4}$$

- For fine structuring at low p_T region,

$$p_{i\perp} \to \xi_i = \log_{10}\left(p_{i\perp}\right) \tag{5}$$

Momentum Space Approach

The lepton helicity-dependent amplitudes for the t-channel diagram is given by:

$$\mathcal{M}^{(t)}_{\lambda_3,\lambda_4} = e\,\mathbf{F_E(q_1)}(p_a+p_1)^\alpha \frac{-ig_{\alpha\mu}}{q_1^2+i\varepsilon}\bar{u}(p_3,\lambda_3)\,i\gamma^\mu \frac{i[(\not{p}_3 - \not{q}_1)+m_l]}{(q_1-p_3)^2-m_l^2}$$
$$\times\, i\gamma^\nu v(p_4,\lambda_4)\frac{-ig_{\nu\beta}}{q_2^2+i\varepsilon}(p_b+p_2)^\beta e\,\mathbf{F_E(q_2)}$$

The u-channel amplitude is:

$$\mathcal{M}^{(u)}_{\lambda_3,\lambda_4} = e\,\mathbf{F_E(q_1)}(p_a+p_1)^\alpha \frac{-ig_{\alpha\mu}}{q_1^2+i\varepsilon}\bar{u}(p_3,\lambda_3)\,i\gamma^\nu \frac{i[(\not{p}_3 - \not{q}_2)+m_l]}{(q_2-p_3)^2-m_l^2}$$
$$\times\, i\gamma^\mu v(p_4,\lambda_4)\frac{-ig_{\nu\beta}}{q_2^2+i\varepsilon}(p_b+p_2)^\beta e\,\mathbf{F_E(q_2)}$$

The total amplitude is the sum of the t- and u-channel contributions:

$$\mathcal{M}_{\lambda_3,\lambda_4} = \mathcal{M}^{(t)}_{\lambda_3,\lambda_4} + \mathcal{M}^{(u)}_{\lambda_3,\lambda_4}$$

Momentum Space Approach

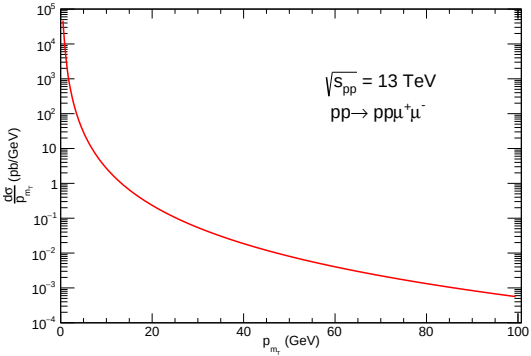

Figure: Differential cross section as a function of $p_{m_T} = p_{t_{\mu^+}} - p_{t_{\mu^-}}$ without any cuts

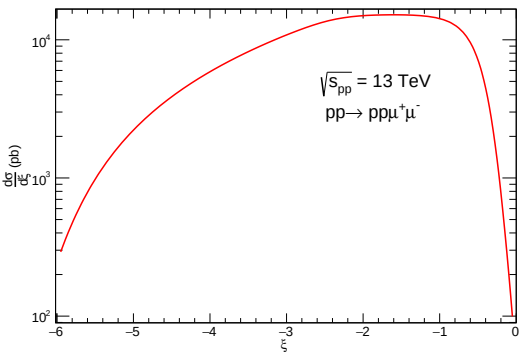

Figure: Differential cross section as a function of $\xi = log_{10}(p_{t_{\mu^\pm}})$ without any cuts

Impact Parameter Space Approach

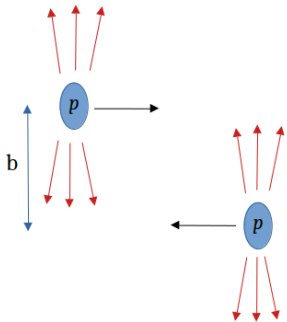

The impact parameter space approach provides GEOMETRICAL CONTROL over the proton-proton collision.

Impact Parameter Space Approach

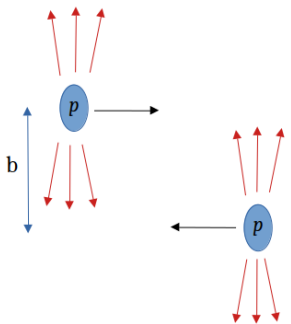

The impact parameter space approach provides GEOMETRICAL CONTROL over the proton-proton collision.

In the Equivalent Photon Approximation, the electromagnetic field of a fast-moving proton is effectively described by a flux of transverse equivalent photons.

Impact Parameter Space Approach

$$n(\omega, b) = \frac{2\alpha}{\pi^2 \omega} \left[\int dq_\perp \, q_\perp^2 \, \frac{F\left(q_\perp^2 + \frac{\omega^2}{\gamma^2}\right)}{q_\perp^2 + \frac{\omega^2}{\gamma^2}} J_1(bq_\perp) \right]^2$$

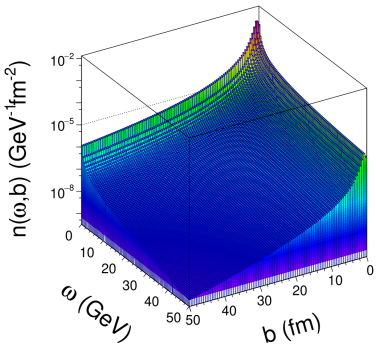

Figure: Equivalent photon flux as a function of ω and b

Impact Parameter Space Approach

$$\sigma(pp \to pp\,\ell^+\ell^-) = \int n(\omega_1, \vec{b}_1)\, n(\omega_2, \vec{b}_2)\, \sigma_{\gamma\gamma\to\ell^+\ell^-}(W_{\gamma\gamma}) \times \frac{W_{\gamma\gamma}}{2}\, d^2\vec{b}_1\, d^2\vec{b}_2\, dW_{\gamma\gamma}\, dY_{\ell^+\ell^-}$$

- $W_{\gamma\gamma}$ – energy in the $\gamma\gamma$ system
- $Y_{\ell^+\ell^-}$ – rapidity of the outgoing lepton pair
- $\vec{b_1}, \vec{b_2}$ - distance to the interaction point from each proton

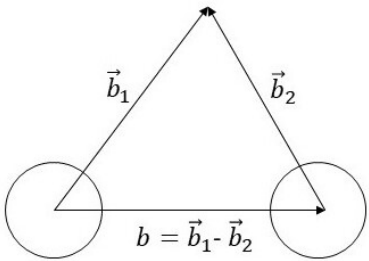

Figure: Schematic view of two protons and transverse distances

Motivation for additional variables: $\bar{b}_x$ and $\bar{b}_y$

$$\sigma(pp \to pp\,\ell^+\ell^-) = \int n(\omega_1, \vec{b}_1)\, n(\omega_2, \vec{b}_2)\, \sigma_{\gamma\gamma\to\ell^+\ell^-}(W_{\gamma\gamma}) \times \frac{W_{\gamma\gamma}}{2}\, 2\pi b\, db\, \bar{b}_x\, \bar{b}_y\, dW_{\gamma\gamma}\, dY_{\ell^+\ell^-}$$

$$\vec{b}_1 = \left(\bar{b}_x + \frac{b}{2},\ \bar{b}_y\right)$$

$$\vec{b}_2 = \left(\bar{b}_x - \frac{b}{2},\ \bar{b}_y\right)$$

- $W_{\gamma\gamma}$: energy in the $\gamma\gamma$ system
- $Y_{\ell^+\ell^-}$: rapidity of the outgoing lepton pair
- b: impact parameter between protons
- $\bar{b}_x$, $\bar{b}_y$: components of $\vec{b}_1$ and $\vec{b}_2$

$$\bar{\mathbf{b}}_\mathbf{x} = \frac{b_{1x} + b_{2x}}{2}, \quad \bar{\mathbf{b}}_\mathbf{y} = \frac{b_{1y} + b_{2y}}{2}$$

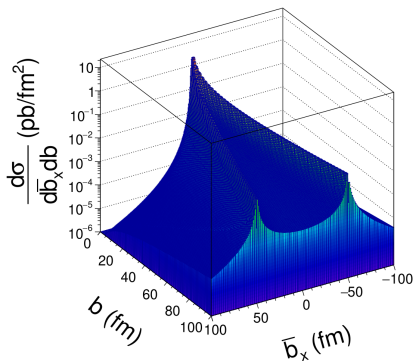

Momentum and Impact Parameter Space Comparison

Calculations in both momentum (p) and impact parameter (b) space are done in phase space $|\eta_\tau| < 3$ for comparison.

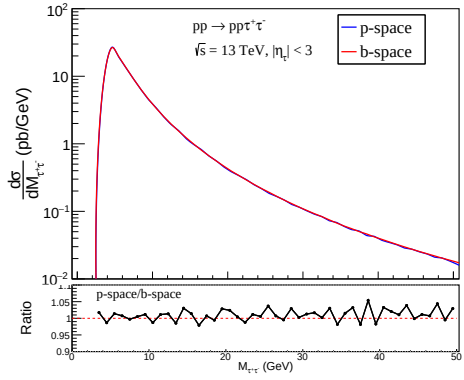

Phase space	σ_{dipole} (pb)
p-space	104.089
b-space	104.543 $\pm$ 0.0074

Figure: Comparison of differential cross section $\frac{d\sigma}{dM}$ for $pp \to pp\tau^+\tau^-$

Effects of changing proton radius

- PDG 2018 proton radius values in the context of radius-puzzle:

Scenario	**B – big proton**	**S – small proton**	**C – conventional**
Proton radius	$r_B = 0.8751$ fm	$r_S = 0.84087$ fm	$r_C = 0.81$ fm
Dipole cut off	$\Lambda_B^2 = 0.6081$ GeV^2	$\Lambda_S^2 = 0.6587$ GeV^2	$\Lambda_C^2 = 0.71$ GeV^2

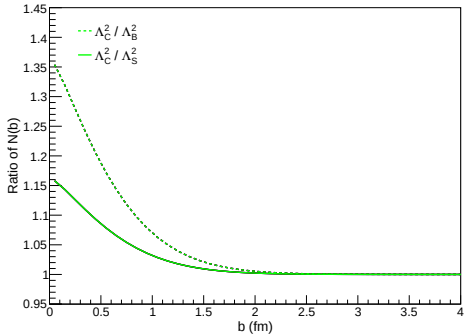

Figure: Ratio of photon flux as a function of impact parameter

Effects of changing proton radius

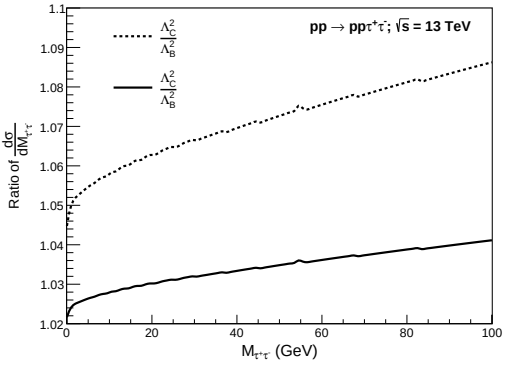

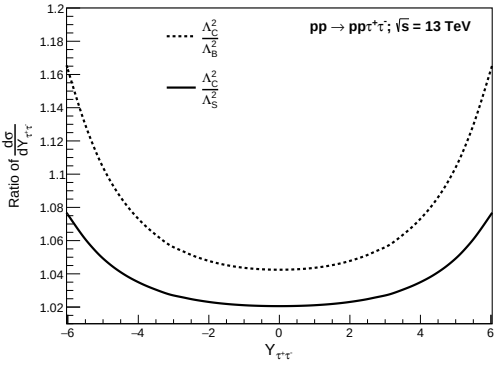

Ratio of (left) $\frac{d\sigma}{dM_{\tau^+\tau^-}}$ and (right) $\frac{d\sigma}{dY_{\tau^+\tau^-}}$ computed with Λ_C^2 to those from PDG radius limits.

Rescattering Corrections

The cross section including rescattering corrections can be written as:

$$\sigma(pp \to pp\,\ell^+\ell^-) = \int n(\omega_1, \vec{b}_1)\, n(\omega_2, \vec{b}_2)\, \sigma_{\gamma\gamma\to\ell^+\ell^-}(W_{\gamma\gamma}) \times S^2_{\gamma\gamma}(\vec{b}) \frac{W_{\gamma\gamma}}{2}\, 2\pi b\, db\, b_x \bar{b}_y\, dW_{\gamma\gamma}\, dY_{\ell^+\ell^-}$$

where the **absorptive factor** is

$$S^2_{\gamma\gamma}(\vec{b}) = \left(1 - e^{-b^2/(2B)}\right)^2$$

and B is the elastic slope parameter, measured by ATLAS:

- $B = 19.73 \pm 0.14$ (stat) ± 0.26 (syst) GeV^{-2} at 7 TeV
- $B = 21.14 \pm 0.13$ GeV^{-2} at 13 TeV

Experimental Comparison

Process & Kinematics	$\sigma_{\text{th}}(\Lambda_C^2)$ (pb)	$\sigma_{\text{th}}(\Lambda_B^2)$ (pb)	σ_{exp} (pb)
LHC at $\sqrt{s} = 7$ TeV			
$pp \to pp\mu^+\mu^-$	0.684 ± 0.000027	0.657 ± 0.000025	$0.628 \pm 0.032 \pm 0.021$
$M_{\mu^+\mu^-} > 20$ GeV, $p_T > 10$ GeV			
$pp \to ppe^+e^-$	0.423 ± 0.000016	0.405 ± 0.000015	$0.428 \pm 0.035 \pm 0.018$
$M_{e^+e^-} > 24$ GeV, $p_T > 12$ GeV			
$pp \to pp\mu^+\mu^-$	3.623 ± 0.00014	3.506 ± 0.00013	$3.38^{+0.58}_{-0.55} \pm 0.21$
$M_{\mu^+\mu^-} > 11.5$ GeV, $p_T > 4$ GeV			
LHC at $\sqrt{s} = 13$ TeV			
$pp \to pp\mu^+\mu^-$	3.373 ± 0.00028	3.266 ± 0.00018	$\mathbf{3.12 \pm 0.07 \pm 0.14}$
$12 < M_{\mu^+\mu^-} < 70$ GeV, $p_T > 6$ GeV			

Comparison of b-space results including the survival factor $S^2_{\gamma\gamma}(b)$ with LHC measurements for Λ_C^2 and Λ_B^2. Data correspond to $\sqrt{s} = 7$ TeV and $\sqrt{s} = 13$ TeV, with **CMS** using $|\eta_{\mu^-}| < 2.1$ and **ATLAS** using $|\eta_{e^-,\mu^-}| < 2.4$.

Experimental Comparison

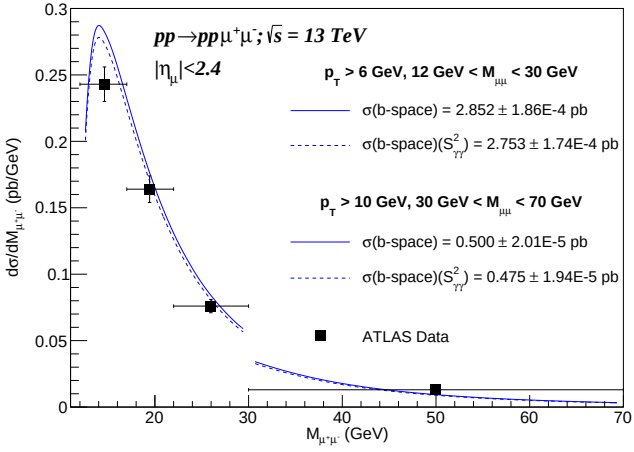

Figure: $d\sigma/dM_{\mu^+\mu^-}$, computed in b-space including survival factor. Results are calculated for ATLAS datasets.

Experimental Sensitivity

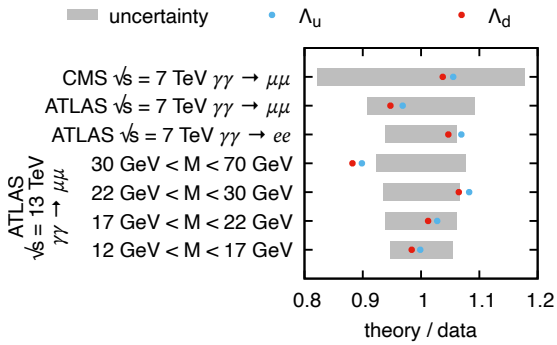

Figure: Ratio of theoretical results with ATLAS and CMS results.

- To quantify experimental sensitivity, performed χ^2 fit test with ATLAS and CMS results.

Experimental Sensitivity

- $\chi^2 = \sum_i \frac{(\sigma_i^{\text{th}} - \sigma_i^{\text{exp}})^2}{\Delta_i^2}$, where Δ_i includes the combined experimental uncertainty.

$$r_p = 0.881 \pm 0.051 \text{ fm}$$
$$\Lambda^2 = 0.599 \pm 0.075 \text{ GeV}^2$$

- The fitted value corresponds to effective dipole radius that reproduces observable kinematic dependence on exclusive dilepton production.

Summary

- Two-photon interactions provide a useful framework to explore the size of the proton.
- $F(Q^2) \rightarrow r_p$
- Better agreement with experiment is obtained for **larger proton size**.
- The impact of varying the proton radius on different kinematical distributions was analyzed.

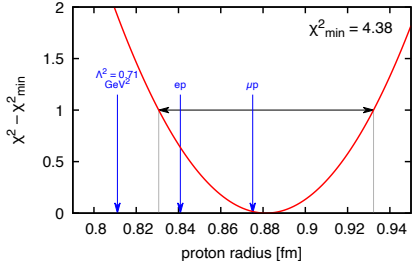

Figure: χ^2 value as a function of proton radius

- Currently investigating the contribution of the magnetic form factor.

THANK YOU VERY MUCH FOR LISTENING

Back up

- For applying experimental cuts, we replace it with a differential form in $z = \cos\theta$:

$$\sigma_{\gamma\gamma\to\ell^+\ell^-}(W_{\gamma\gamma}) \quad \longrightarrow \quad \frac{d\sigma_{\gamma\gamma\to\ell^+\ell^-}}{dz}(W_{\gamma\gamma}, z)$$

- This allows us to impose experimental cuts on kinematic variables for individual leptons

$$E_{\ell^\pm} = \frac{W_{\gamma\gamma}}{2}$$

$$p_{\ell^\pm} = \sqrt{\left(\frac{W_{\gamma\gamma}}{2}\right)^2 - m_\ell^2}$$

$$p_z = z \cdot p$$

$$p_T = \sqrt{1 - z^2} \cdot p$$

$$y_{\ell^\pm} = Y_{\ell^+\ell^-} \pm y_{\ell^\pm/\ell^+\ell^-}(W_{\gamma\gamma}, z)$$